

Topologically distinct critical theories emerging from the bulk entanglement spectrum of integer quantum Hall states on a lattice

Qiong Zhu¹, Xin Wan¹, and Guang-Ming Zhang^{2,3}

¹*Zhejiang Institute of Modern Physics, Zhejiang University, Hangzhou 310027, China*

²*State Key Laboratory of Low-Dimensional Quantum Physics and
Department of Physics, Tsinghua University, Beijing 100084, China*

³*Collaborative Innovation Center of Quantum Matter, Beijing, China*

(Dated: December 7, 2024)

The critical theories for the topological phase transitions of integer quantum Hall states to a trivial insulating state with the same symmetry can be obtained by calculating the ground state entanglement spectrum under a symmetric checkerboard bipartition. In contrast to the gapless edge excitations under the left-right bipartition, a quantum network with bulk gapless excitations naturally emerges at the Brillouin zone center without fine tuning. On a large finite lattice, the resulting critical theory for the $\nu = 1$ state is the (2+1) dimensional relativistic quantum field theory characterized by a *single* Dirac cone spectrum and a pair of *fractionalized* zero-energy states, while for the $\nu = 2$ state the critical theory exhibits a parabolic spectrum and no sign of fractionalization in the zero-energy states. A triangular correspondence is established among the bulk topological theory, gapless edge theory, and the critical theory via the ground state entanglement spectrum.

PACS numbers: 73.43.Cd, 73.43.Nq, 03.67.Mn

Introduction.— The integer quantum Hall (IQH) effect has been well studied in various two-dimensional (2D) electron systems, including the experimental observation in graphene[1, 2]. When the time reversal symmetry is broken, the 2D electron systems are characterized by a topological quantum number known as the Chern number[3], which can be measured experimentally as the quantized Hall conductance with high precision[4]. In 1988, Haldane[5] proposed a famous honeycomb lattice model for the IQH effect, which allows the access to the phase transition between the pure Hall state ($\nu = 1$) and its trivial insulating state ($\nu = 0$) through tuning the time-reversal symmetry or inversion symmetry breaking parameters. Such a transition is a prototype of topological quantum phase transition. Unlike the Landau-Ginzberg-Wilson paradigm for the symmetry breaking phase transitions, the quantum criticality is characterized by the Dirac spectrum with the parity anomaly and undoubled chiral fermions in the lattice realization of the (2+1)D relativistic quantum field theory[5, 6]. Moreover, interesting features can arise in the phase transitions for the $\nu > 1$ IQH states, e.g., charge carriers with the parabolic energy spectrum in pristine bilayer graphene exhibit distinct features with a double-step transition[7]. Therefore, a systematic method is called for to study the critical properties of the 2D topological phases.

It is generally believed that the essential information of a topological phase is encoded in its ground state wave function. Li and Haldane[8] introduced entanglement spectrum as the collection of eigenvalues of the reduced density matrix under a left-right bipartition, and found that the low-lying spectrum bears a remarkable similarity to the physical edge spectrum of the topological state[9–12]. A further step is to ask how one can extract the bulk critical properties for the transition from the topo-

logical phase to its trivial insulating phase with the same symmetry, and what the relationship is between the corresponding gapless edge theory and the bulk critical theory.

In fact, the critical theory can be regarded as the “domain wall” between the topological phase and its trivial insulating phase in the parameter space, hence realizing delocalized boundary excitations of the non-trivial topological phase[13]. To reveal such a non-trivial quantum criticality, appropriated boundary conditions are needed. For the IQH transitions, the domains of trivial and non-trivial phases described by a Dirac Hamiltonian with respective positive and negative masses[5, 6] must be adjacent to each other in the model for the critical theory. Accordingly, the edge modes along the boundaries of the domains form a percolating network. As Haldane pointed out[5], along the critical line between the trivial and topological phases, one expects a low-lying massless Dirac spectrum. Hsieh and Fu[14] argued that a symmetric extended bipartition of the system into two subsystems as long as the size of the sublattice unit cell is larger than the correlation length of the topological phase can realize such boundary conditions.

In this paper we show that the critical theories for the topological phase transitions for IQH states defined on a two-dimensional square lattice can be obtained by calculating the ground state entanglement spectrum under a symmetric checkerboard bipartition. A quantum network with gapless bulk excitations naturally emerges at the Brillouin zone center without any tuning parameters. The critical theory for the $\nu = 1$ state is the (2+1)-dimensional relativistic quantum field theory characterized by a single Dirac cone spectrum and a pair of fractionalized zero-energy states, while for the $\nu = 2$ state the critical theory has a parabolic spectrum and

exhibits no sign of fractionalization in the zero-energy states. Hence, we expect two distinct types of IQH transitions, as observed in monolayer graphene[1, 2, 15] and bilayer graphene[7, 16], respectively. Based on the bulk-edge correspondence of a topological phase, a generic triangular correspondence among the bulk topological theory, gapless edge excitations, and the bulk critical theory is thus established via the ground state entanglement spectrum.

Model and method.- We consider a tight-binding Hamiltonian on a 2D square lattice in the presence of a perpendicular magnetic field,

$$H = - \sum_{\langle ij \rangle} \left(e^{i\theta_{ij}} c_i^\dagger c_j + h.c. \right), \quad (1)$$

where the total phase that an electron picks up when moving around a plaquette

$$\sum_{\square} \theta_{ij} = 2\pi \frac{\phi}{\phi_0} \quad (2)$$

is given by the magnetic flux ϕ per unit cell, in units of magnetic flux quantum $\phi_0 = hc/e$. The energy spectrum of the system exhibits a self-similar pattern, known as the Hofstadter butterfly[17]. We first focus on the case of $\phi/\phi_0 = 1/3$, at which the tight-binding band is split into three magnetic subbands, which carry Chern numbers $\nu = 1, -2$, and 1 , respectively. Figure 1(a) shows the density of states from a 300×300 square lattice. With the open boundary condition in the y direction, the corresponding spectrum includes chiral edge states in the two band gaps, as illustrated in Fig. 1(b). Actually the tight-binding Hamiltonian can describe a lattice realization of the Landau levels and the subsequent IQH transitions. The topological phases belong to the class A in the classification of noninteracting topological insulators/superconductors[18]. The time-reversal symmetry is explicitly broken by the external magnetic flux, which determines the propagation direction of the chiral edge modes.

The presence of the chiral edge modes in the topological system is an example of the so-called bulk-edge correspondence. It also manifests at the artificial boundary in the study of quantum entanglement[8]. After we fill up the lowest magnetic subband in the case of $\phi = \phi_0/3$, the Fermi energy lies in the spectral gap and the system is in the $\nu = 1$ IQH phase. If we cut a square A in the bulk of the system and trace out all the degrees of freedom in area B outside the square in the density matrix of the ground state Ψ_0 , the spectrum of the resulting reduced density matrix $\rho_A = \text{Tr}_B(|\Psi_0\rangle\langle\Psi_0|)$ resembles the energy spectrum of a chiral Fermi liquid, which is described by a (1+1)D chiral massless Dirac fermion field theory. Heuristically, we can represent such a bipartition by a directed loop surrounding A.

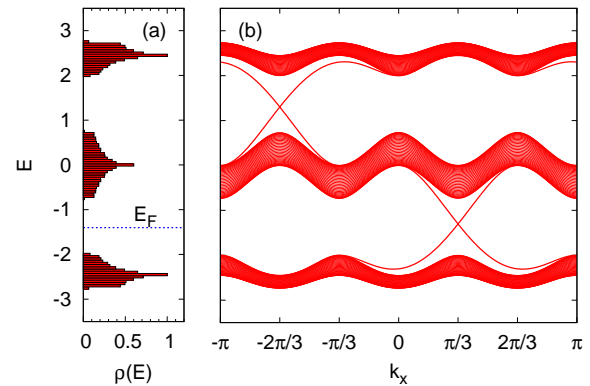


FIG. 1: (Color online) (a) Density of states of the tight-binding 300×300 lattice model with periodic boundary conditions. (b) Corresponding dispersion curves with open boundary condition in y -direction only.

The technique on computing the spectrum of the reduced density matrix for non-interacting systems has been well documented in the literature[19]. The key lies in the computation of the correlation matrix $g_{ij} = \langle c_i^\dagger c_j \rangle$ in the ground state, where i, j denote the lattice sites in the subsystem A. The correlation matrix is isospectral to the reduced density matrix $\rho_A \equiv e^{-H_E}$ or the entanglement Hamiltonian H_E . For a non-interacting electron system, the entanglement Hamiltonian takes a quadratic form

$$H_E = \sum_{n,m} h_{nm} c_n^\dagger c_m. \quad (3)$$

More precisely, g_{ij} encodes the Fermi-Dirac distribution function for the eigenstates of H_E such that the eigenvalues of g_{ij} are expressed as $\eta_l = 1/(e^{\varepsilon_l} + 1)$, in which ε_l s are the eigenvalues of H_E , or the energy levels of the ground state entanglement spectrum. As usual, the states with negative ε_l are occupied.

Emergence of a single Dirac cone.- To reveal the information beyond the edge properties of the IQH $\nu = 1$ state, we implement the symmetric checkerboard bipartition of a finite lattice[14], as illustrated in Fig. 2(a). Heuristically, the remaining half of the square blocks supports chiral edge modes (one per block) represented by directed loops, which form a regular lattice with the unit cell twice the size of the block and rotated by $\pi/4$. With quantum tunneling at the block corners, the loops coalesce into a regular network. If we further assign random tunneling amplitudes at the corners, we will obtain the Chalker-Cottingham network model[20], which can describe the generic IQH plateau transition.

Figure 2(b) plots the spectrum of the entanglement Hamiltonian H_E for a large square lattice with a linear size $L = 300$. Here, we choose each block in part A or B to include 3×3 sites, or a total magnetic flux $3\phi_0$.

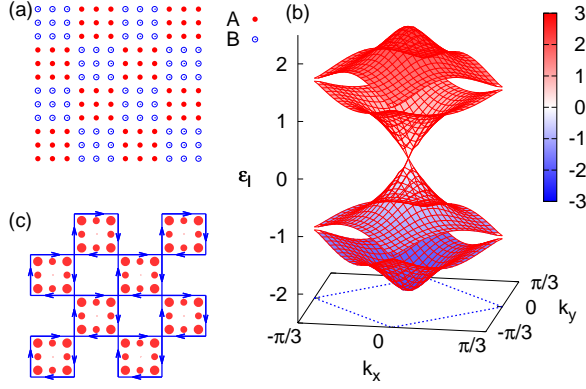


FIG. 2: (Color online) (a) Symmetric checkerboard bipartition illustrated in a 12×12 lattice. (b) Spectrum of the entanglement Hamiltonian H_E . For the clarity of the Dirac spectrum centered at $k = (0, 0)$ and $\epsilon_l = 0$, we only plot the four bands with energies closest to zero. The Brillouin zone corresponding to the checkerboard lattice is illustrated by the blue square. (c) The total probability density of the two zero-energy states in the finite 12×12 lattice, whose chiral edge-state nature is represented by the directed loops. The area of each dot is proportional to the local probability density.

For clarity, we only plot the four bands (out of nine) closest to zero in the entanglement spectrum. The most remarkable feature of the spectrum is the single Dirac cone appearing at the Brillouin zone center. The emergent entanglement spectrum hence differs qualitatively from the energy spectrum of the original lattice model. For comparison, we note that the Hamiltonian (1) with $\phi = \phi_0/2$ has two Dirac cones in its energy spectrum that usually appears in lattice realizations of the (2+1)D relativistic quantum field theories. The defeat of the fermion doubling here is rooted both in the broken time-reversal symmetry of the original lattice model and in the broken 2D parity symmetry due to the checkerboard bipartition. Accordingly, the bipartition generates a non-interacting Hamiltonian H_E on the non-simply connected 2D sublattice A with long-range ($\sim 1/r$) complex hopping amplitudes.

At the Dirac cone vertex, there *always* exist two degenerate zero-energy states, regardless of the different sizes of the lattice system and the block size for the checkerboard bipartition; the Kramers degeneracy is the consequence of the emergent time-reversal symmetry of the low-energy effective Dirac Hamiltonian $H_1 = \alpha \sigma \cdot \mathbf{p}$ [6]. We plot the *total* probability density of the zero-energy states in Fig. 2(c) by filled circles. In each 3×3 block the density retains the point-group symmetry of the lattice and the center site in each block has zero density. This is a striking manifestation of the constituting edge mode within each block. With the directed loops attached around the blocks, we emphasize the emergence of the disorder-free Chalker-Cottingham network

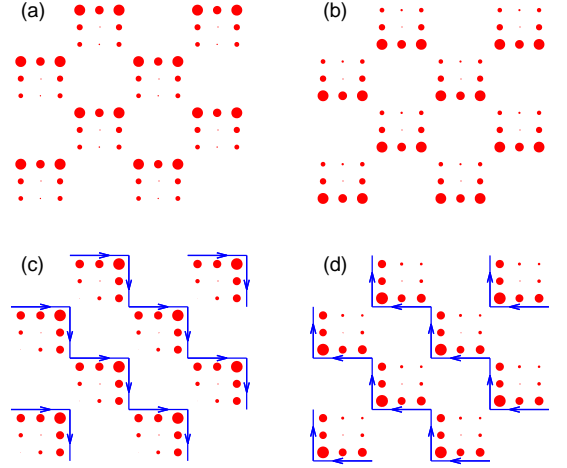


FIG. 3: (Color online) (a) and (b) The probability densities (proportional to the area of the dots) of the two zero-energy states (we only show a 12×12 sector for clarity). The probability is significant on half of the edge sites from each block only. (c) and (d) The probability densities of the two zero-energy states in (a) and (b) after a rotation of $\pi/8$ in their spinor representation. The sites with significant probability density follow chiral stairs either up or down.

picture[20], which can be mapped to the Dirac Hamiltonian in 2D system[21]. In fact, the eigenstates of the whole Dirac cone are linear combinations of the edge modes of individual blocks.

Fractionalization of zero-energy states.— The single Dirac cone structure in the entanglement spectrum also demonstrates that the low-energy effective Hamiltonian H_1 has a particle-hole symmetry, which is not present in the original lattice model[5, 6]. A further consequence is the charge fractionalization due to the parity anomaly of the (2+1)D effective field theory[22]. We have carefully studied this two-dimensional space spanned by the zero-energy states at the Dirac cone vertex by plotting their separate probability densities. As illustrated in Fig. 3(a) and (b), the fractionalization manifests in a way that either state is formed by the significant occupations on only *half* of the edge sites in each block. The fractionalization cannot be removed by any linear combinations of the two states, which only rotate the probability density around the edge in each block simultaneously.

The fractionalization of the edge degrees of freedom of each block is consistent with the fact that the Dirac cone emerges at the center of the Brillouin zone, hence representing the long-wavelength collective behavior of the system. By a $\pi/8$ -rotation of the zero-energy states in their spinor representation, the probability densities rotate $\pi/4$ in the real space along the edge of each block, and we effectively fractionalize the network model as in Fig. 3(c) and (d). One state has the probability density essentially on the edges marked by right and down

arrows, while the other by left and up ones. They form chiral, coherent, and penetrating paths across the system along the diagonal direction. The features of the fractionalization become more prominent as we increase the block size in each sublattice, which allows a cleaner separation of the bulk and the edge of each block. According to the Jackiw argument[22], the charge conjugation symmetry leads to a quantum Hall effect at $\nu = 1/2$ with the zero-energy states filled and at $\nu = -1/2$ with them empty.

Topologically distinct transitions.- The low-lying massless spectrum of the undoubled chiral fermions and the parity anomaly confirms that the phase transition from the $\sigma_{xy} = e^2/h$ IQH state to a band insulator can emerge from the entanglement spectrum of the ground state wave function in the non-trivial phase. In unspecific words, we can unveil the full information of the gapless critical point from the wave function on the topological side. To support the general statement, we continue to explore the emergent physics under the checkerboard bipartition for the IQH state with $\sigma_{xy} = 2e^2/h$.

In Figure 4(a), we plot the entanglement spectrum in a $\phi = \phi_0/9$ system with the lowest two magnetic subbands filled, which is a topological state with $\sigma_{xy} = 2e^2/h$. In contrast to the Dirac cone spectrum in the $\sigma_{xy} = e^2/h$ case, we find that undoubled chiral fermions with a parabolic dispersion at the Brillouin zone center associated with a Berry flux of 2π . In addition, a pair of adjacent bands [red lines in Fig. 4(a)] is also visible with a gap opened at the Brillouin center. The band structure, together with the earlier $\sigma_{xy} = e^2/h$ case, reminds us of the spectral difference between monolayer and pristine bilayer graphene[15], except that the graphene systems have two valleys at the two inequivalent corners of their hexagonal Brillouin zone. In our case, the parabolic low-energy spectrum emerges at the zone center without fine tuning. The four bands can be regarded as resulting from the reconstruction of the two Dirac cones which one may naively expect to appear at the zone center, if one asserts that no quantum entanglement exists between states in different subbands separated by a spectral gap. The existence of the quadratic band-crossing point is allowed due to the emergent time-reversal symmetry and the C_4 lattice symmetry[23]. Like graphene, we find that the distinction of the $\sigma_{xy} = e^2/h$ and $2e^2/h$ cases lies in the Berry flux (π and 2π , respectively) of the chiral fermions[16]. Therefore, the emergent spectrum describes a double-step transition from the $\sigma_{xy} = 2e^2/h$ IQH state to the corresponding $\sigma_{xy} = 0$ state, much like the double-step IQH transition in bilayer graphene[7].

The fractionalization of the zero-energy states is the hallmark of the (2+1)D relativistic quantum field theory, hence ought to be absent in the $\sigma_{xy} = 2e^2/h$ case. We plot the probability densities of the two zero-energy states in Fig. 4(b) and (c). As was pointed out earlier, the densities are mostly distributed along the block edges.

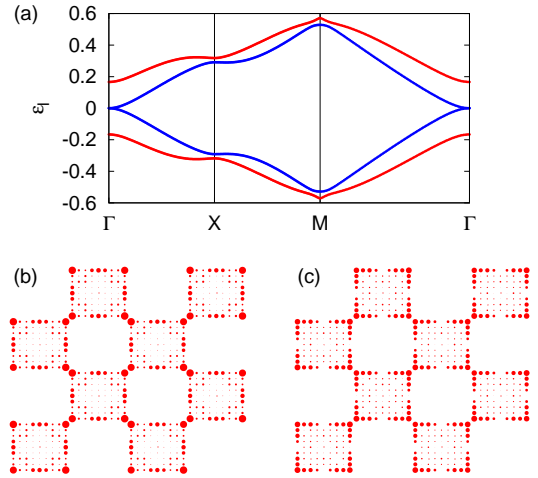


FIG. 4: (Color online) (a) Dispersion curves of the entanglement spectrum from the checkerboard bipartition (in 9×9 blocks) with $\phi = \phi_0/9$ and two magnetic subbands filled. (b) and (c) The probability densities (proportional to the area of the dots) of the two zero-energy states.

However, we find no sign of fractionalization as in the earlier case, even though we exhaust all linear combinations of the states, which only lead to the probability density transfer between the corners and the edges (somewhat like breathing).

We further study the IQH states with $\nu > 2$. For example, four Dirac points with Berry flux π and one additional Dirac point with flux $-\pi$ can appear for $\nu = 3$, and four Dirac points with Berry flux π can appear for $\nu = 4$, which are consistent with the C_4 lattice symmetry. In general, the number of the Dirac cones can be affected by the reconstruction of the entanglement spectrum, but the associated Berry flux cannot. In other words, the Berry flux for the ground state wave function of the entanglement Hamiltonian provides a topological \mathbb{Z} classification of the transitions from the original IQH states to the trivial one.

Conclusion and outlook.- We have shown that the critical theory between the topological state and the corresponding trivial state can emerge in the entanglement spectrum of the non-trivial state with a symmetric checkerboard bipartition. The bipartition generates a quantum network with gapless bulk excitations. The critical theories for topologically different systems can be distinguished by the behavior of the low-energy entanglement spectrum and its degenerate zero-energy states. The IQH states to an insulator transitions we discussed here are in the clean limit, which may be tuned by an additional periodic potential[24]. Distinct effects of quenched disorder may be considered separately.

Remarkably, the ground state wave function of the topological bulk theory encodes not only the boundary theory[8], but also the critical theory for its transition

to a trivial insulator with the same symmetry, both of which can be derived from the ground state entanglement spectrum under different types of bipartitions[14, 25–27]. Therefore, we can expect a generic triangular correspondence among the bulk topological theories, the gapless edge theories, and the bulk critical theories. The edge theories is the critical theories spatially confined between the topological phases and the trivial insulating phases, while the percolating quantum networks of the edge modes establish the critical theories for the transitions of the topological phases to the trivial phases.

Moreover, the time-reversal symmetry of the lattice model can be restored by including two copies of $\nu = 1$ IQH states with opposite spin indices, which is topologically distinct from the time-reversal symmetry breaking $\nu = 2$ IQH state. This is the simplest realization of quantum spin Hall state[28]. In this case, two degenerate Dirac cones are expected in the entanglement spectrum under the symmetric checkerboard bipartition, describing the topological phase transition of the quantum spin Hall state to a normal insulator. The corresponding four degenerate zero-energy modes can be separated into fractionalized charge and spin collective excitation modes. More exotic structures of the entanglement spectrum can emerge when the particle-hole symmetry is supplemented in the original model, especially in the case of $p + ip$ superconductors[29].

One of the authors (XW) would like to thank M.-C. Chung for many valuable discussions on the entanglement spectrum in free lattice models. The authors acknowledge the support of the 973 Program under Project No. 2012CB927404 and of NSF-China through the grants No. 20121302227 and No. 11174246.

-
- [1] K. S. Novoselov *et al.*, Nature **438**, 197 (2005).
 - [2] Y. Zhang, J. W. Tan, H. L. Stormer, and P. Kim, Nature **438**, 201 (2005).
 - [3] D. J. Thouless, M. Kohmoto, M. P. Nightingale, and M. den Nijs, Phys. Rev. Lett. **49**, 405 (1982).
 - [4] K. von Klitzing, G. Dorda, and M. Pepper, Phys. Rev. Lett. **45**, 494 (1980).
 - [5] F. D. M. Haldane, Phys. Rev. Lett. **61**, 2015 (1988).
 - [6] A. W. W. Ludwig, M. P. A. Fisher, R. Shankar, and G. Grinstein, Phys. Rev. B **50**, 7526 (1994).
 - [7] K. S. Novoselov, *et al.*, Nature Phys. **2**, 177 (2006).
 - [8] H. Li and F. D. M. Haldane, Phys. Rev. Lett. **101**, 010504 (2008).
 - [9] R. Thomale, A. Sterdyniak, N. Regnault, and B. A. Bernevig, Phys. Rev. Lett. **104**, 180502 (2010).
 - [10] A. Chandran, M. Hermanns, N. Regunault, and B. A. Bernevig, Phys. Rev. B **84**, 205136 (2011).
 - [11] X. L. Qi, H. Katsura, and A. W. W. Ludwig, Phys. Rev. Lett. **108**, 196402 (2012).
 - [12] V. Alba, M. Haque, and A. M. Lauchli, Phys. Rev. Lett. **108**, 227201 (2012).
 - [13] X. Chen, F. Wang, Y. M. Lu, and D. H. Lee, Nucl. Phys. B **873**, 248 (2013).
 - [14] T. H. Hsieh and L. Fu, Phys. Rev. Lett. **113**, 106801 (2014).
 - [15] A. H. Castro Neto, F. Guinea, N. M. R. Peres, K. S. Novoselov, and A. K. Geim, Rev. Mod. Phys. **81**, 109 (2009).
 - [16] E. McCann and V. I. Fal’ko, Phys. Rev. Lett. **96**, 086805 (2006).
 - [17] D. R. Hofstadter, Phys. Rev. B **14**, 2239 (1976).
 - [18] A. P. Schnyder *et al.*, Phys. Rev. B **78**, 195125 (2008); A. Kitaev, AIP Conf. Proc. **1134**, 22 (2009).
 - [19] For a review, see I. Peschel and V. Eisler, J. Phys. A: Math. Theor. **42**, 504003 (2009).
 - [20] J. T. Chalker and P. D. Coddington, J. Phys. C **21**, 2665 (1988).
 - [21] C. M. Ho and J. T. Chalker, Phys. Rev. B **54**, 8708 (1996).
 - [22] R. Jackiw, Phys. Rev. D **29**, 2375 (1984).
 - [23] K. Sun, H. Yao, E. Fradkin, and S. A. Kivelson, Phys. Rev. Lett. **103**, 046811 (2009).
 - [24] X. G. Wen and Y. S. Wu, Phys. Rev. Lett. **70**, 1501 (1993); W. Chen, M. P. A. Fisher, and Y. S. Wu, Phys. Rev. B **48**, 13749 (1993).
 - [25] W. J. Rao, X. Wan, and G. M. Zhang, Phys. Rev. B **90**, 075151 (2014).
 - [26] T. H. Hsieh, L. Fu, and X. L. Qi, Phys. Rev. B **90**, 085137 (2014).
 - [27] R. A. Santos, arXiv:1408.1716 (unpublished).
 - [28] C. L. Kane and E. J. Mele, Phys. Rev. Lett. **95**, 146802 (2005); B. A. Bernevig and S. C. Zhang, Phys. Rev. Lett. **96**, 106802 (2006).
 - [29] N. Read and D. Green, Phys. Rev. B **61**, 10267 (2000).